



## OPEN ACCESS

## EDITED BY

Min Wu,  
Sichuan University, China

## REVIEWED BY

Chuoji Huang,  
Macau University of Science and  
Technology, China  
Ahmad Umar Khan,  
Teerthanker Mahaveer University, India

## \*CORRESPONDENCE

Peng Zhou  
penghyzhou@126.com

<sup>†</sup>These authors have contributed  
equally to this work and share  
first authorship

## SPECIALTY SECTION

This article was submitted to  
Cancer Imaging and  
Image-directed Interventions,  
a section of the journal  
Frontiers in Oncology

RECEIVED 25 August 2022

ACCEPTED 26 September 2022

PUBLISHED 06 October 2022

## CITATION

He C, Liu J, Li Y, Lin L, Qing H, Guo L,  
Hu S and Zhou P (2022) Quantitative  
parameters of enhanced dual-energy  
computed tomography for  
differentiating lung cancers from  
benign lesions in solid  
pulmonary nodules.  
*Front. Oncol.* 12:1027985.  
doi: 10.3389/fonc.2022.1027985

## COPYRIGHT

© 2022 He, Liu, Li, Lin, Qing, Guo, Hu  
and Zhou. This is an open-access article  
distributed under the terms of the  
[Creative Commons Attribution License  
\(CC BY\)](https://creativecommons.org/licenses/by/4.0/). The use, distribution or  
reproduction in other forums is  
permitted, provided the original  
author(s) and the copyright owner(s)  
are credited and that the original  
publication in this journal is cited, in  
accordance with accepted academic  
practice. No use, distribution or  
reproduction is permitted which does  
not comply with these terms.

# Quantitative parameters of enhanced dual-energy computed tomography for differentiating lung cancers from benign lesions in solid pulmonary nodules

Changjiu He<sup>†</sup>, Jieke Liu<sup>†</sup>, Yong Li, Libo Lin, Haomiao Qing,  
Ling Guo, Shibe Hu and Peng Zhou\*

Department of Radiology, Sichuan Cancer Hospital & Institute, Sichuan Cancer Center, School of Medicine, University of Electronic Science and Technology of China, Chengdu, China

**Objectives:** This study aimed to investigate the ability of quantitative parameters of dual-energy computed tomography (DECT) and nodule size for differentiation between lung cancers and benign lesions in solid pulmonary nodules.

**Materials and Methods:** A total of 151 pathologically confirmed solid pulmonary nodules including 78 lung cancers and 73 benign lesions from 147 patients were consecutively and retrospectively enrolled who underwent dual-phase contrast-enhanced DECT. The following features were analyzed: diameter, volume, Lung CT Screening Reporting and Data System (Lung-RADS) categorization, and DECT-derived quantitative parameters including effective atomic number (Zeff), iodine concentration (IC), and normalized iodine concentration (NIC) in arterial and venous phases. Multivariable logistic regression analysis was used to build a combined model. The diagnostic performance was assessed by area under curve (AUC) of receiver operating characteristic curve, sensitivity, and specificity.

**Results:** The independent factors for differentiating lung cancers from benign solid pulmonary nodules included diameter, Lung-RADS categorization of diameter, volume, Zeff in arterial phase (Zeff\_A), IC in arterial phase (IC\_A), NIC in arterial phase (NIC\_A), Zeff in venous phase (Zeff\_V), IC in venous phase (IC\_V), and NIC in venous phase (NIC\_V) (all  $P < 0.05$ ). The IC\_V, NIC\_V, and combined model consisting of diameter and NIC\_V showed good diagnostic performance with AUCs of 0.891, 0.888, and 0.893, which were superior to the diameter, Lung-RADS categorization of diameter, volume, Zeff\_A, and Zeff\_V (all  $P < 0.001$ ). The sensitivities of IC\_V, NIC\_V, and combined model were higher than those of IC\_A and NIC\_A (all  $P < 0.001$ ). The combined model did not increase the AUCs compared with IC\_V ( $P = 0.869$ ) or NIC\_V ( $P = 0.633$ ).

**Conclusion:** The DECT-derived IC\_V and NIC\_V may be useful in differentiating lung cancers from benign lesions in solid pulmonary nodules.

KEYWORDS

dual-energy computed tomography, iodine concentration, solid pulmonary nodule, lung cancer, benign lesion

## Introduction

Lung cancer is the leading cause of cancer-induced death worldwide (1–3). With the popularization of lung cancer screening and computed tomography (CT), the detection rate of pulmonary nodules has been greatly improved (4). Now the Lung CT Screening Reporting and Data System (Lung-RADS) is widely used to assess and manage pulmonary nodules according to the nodule size (5, 6), as the malignancy probability of a given nodule increases with its size (7). However, previous studies demonstrated that the Lung-RADS categorization had insufficient diagnostic accuracy for distinguishing lung cancers from benign lesions appearing as solid pulmonary nodules (8, 9). The relatively low specificity of the Lung-RADS categorization may lead to excessive diagnosis and treatment of benign nodules (9, 10). Besides, radiologists usually evaluate the risk of pulmonary nodules by interpreting the morphological characteristics on chest CT. But there is an overlap of morphological findings between malignant and benign nodules (11), as non-calcified granulomas also tend to present with malignant signs of lobulation or spiculation (12, 13). Therefore, it is still a challenge for radiologist to differentiate lung cancers from benign solid pulmonary nodules.

Dual-energy computed tomography (DECT) has advantages in chest imaging by providing multiple quantitative parameter such as iodine concentration (IC) and effective atomic number (Zeff). It also can reduce the use of required contrast agent and the radiation dose by omitting a true unenhanced CT (14). Previous studies demonstrated that IC or normalized iodine concentration (NIC) could differentiate lung cancers from inflammation (15, 16) and differentiate malignant from benign solitary pulmonary nodules (17–19). All these studies only investigated the quantitative parameters that were related to iodine and enhancement, however, neglected the role of nodule size. Besides, solid and subsolid nodules were not separately examined in most studies (15–17, 19). One of them reported that 18 of 33 solid nodules were malignant while 16 of 16 subsolid nodules were adenocarcinomas (19), which was similar to the results of large cohorts (20, 21). Hence the DECT studies in subsolid nodules focused on the differentiation of invasiveness of adenocarcinomas rather than that between lung cancers and benign lesions (22, 23).

Therefore, this study aimed to investigate the ability of quantitative parameters of DECT for differentiation between lung cancers and benign lesions in solid pulmonary nodules, and compare their diagnostic performance with nodule size and Lung-RADS.

## Materials and methods

### Patients

This study was approved by the Institutional Review Board of Sichuan Cancer Hospital, and the written informed consent was obtained from all participants. A total of 580 consecutive pulmonary nodules were preliminarily enrolled from the Sichuan Cancer Hospital from April 2020 to November 2021. The inclusion criteria were as following: patients with dual-phase contrast-enhanced chest DECT, patients with solid pulmonary nodules (diameter < 3 cm), and histopathologic diagnosis *via* surgical resection. The exclusion criteria were as following: subsolid nodules (n = 414, 378 lung cancers and 36 benign lesions), with cancer history in previous 5 years (n = 2), receiving anti-cancer treatment prior to DECT (n = 10), unsatisfactory image quality due to respiratory and movement artifacts (n = 3).

A total of 151 solid pulmonary nodules including 78 lung cancer (69 adenocarcinomas, 6 squamous cell carcinomas, and 3 small cell lung carcinoma) and 73 benign lesions (34 inflammations, 24 granulomas, 10 benign tumors, and 5 other benign entities) from 147 patients were finally enrolled in this study (Table 1) (Figure 1).

### Image acquisition

All DECT scans were performed on a second-generation dual-source CT (Somatom Definition Flash, Siemens Healthcare, Forchheim, Germany). A total of 90 ml contrast medium (370 mg iodine/mL, Iopromide, Bayer, Guangzhou, China) was injected *via* an antecubital vein at a flow rate of 3.0 mL/s, and followed by 30 ml of physiological saline at the same

TABLE 1 The characteristics of solid pulmonary nodules.

| Characteristics            | Lung cancer (n=78) | Benign lesion (n=73) | P       |
|----------------------------|--------------------|----------------------|---------|
| Histologic subtype         |                    |                      |         |
| Adenocarcinomas            | 69                 |                      |         |
| Squamous cell carcinomas   | 6                  |                      |         |
| Small cell lung carcinomas | 3                  |                      |         |
| Inflammations              |                    |                      |         |
| Granulomas                 |                    | 34                   |         |
| Benign tumors              |                    | 24                   |         |
| Other benign entities      |                    | 10                   |         |
| Gender                     |                    | 5                    | 0.194   |
| Female                     | 43                 | 32                   |         |
| Male                       | 35                 | 41                   |         |
| Age (years)                | 57.9 ± 10.9        | 55.5 ± 11.3          | 0.189   |
| Diameter (mm)              | 16.7 ± 6.1         | 14.2 ± 6.3           | 0.013   |
| Lung-RADS (diameter)       |                    |                      |         |
| 2                          | 2                  | 4                    | 0.008   |
| 3                          | 3                  | 9                    |         |
| 4A                         | 25                 | 34                   |         |
| 4B or 4X                   | 48                 | 26                   |         |
| Volume (cm <sup>3</sup> )  | 4.187 ± 4.160      | 2.869 ± 3.399        | 0.036   |
| Lung-RADS (volume)         |                    |                      |         |
| 2                          | 0                  | 3                    | 0.050   |
| 3                          | 5                  | 6                    |         |
| 4A                         | 22                 | 30                   |         |
| 4B or 4X                   | 51                 | 34                   |         |
| Zeff_A                     | 8.07 ± 0.68        | 7.73 ± 0.49          | 0.001   |
| IC_A (mg/mL)               | 1.43 ± 0.86        | 0.59 ± 1.43          | < 0.001 |
| NIC_A (%)                  | 13.46 ± 8.25       | 5.54 ± 13.28         | < 0.001 |
| Zeff_V                     | 8.42 ± 0.56        | 7.84 ± 1.01          | < 0.001 |
| IC_V (mg/mL)               | 2.03 ± 0.76        | 0.68 ± 0.97          | < 0.001 |
| NIC_V (%)                  | 36.74 ± 13.49      | 11.92 ± 17.85        | < 0.001 |

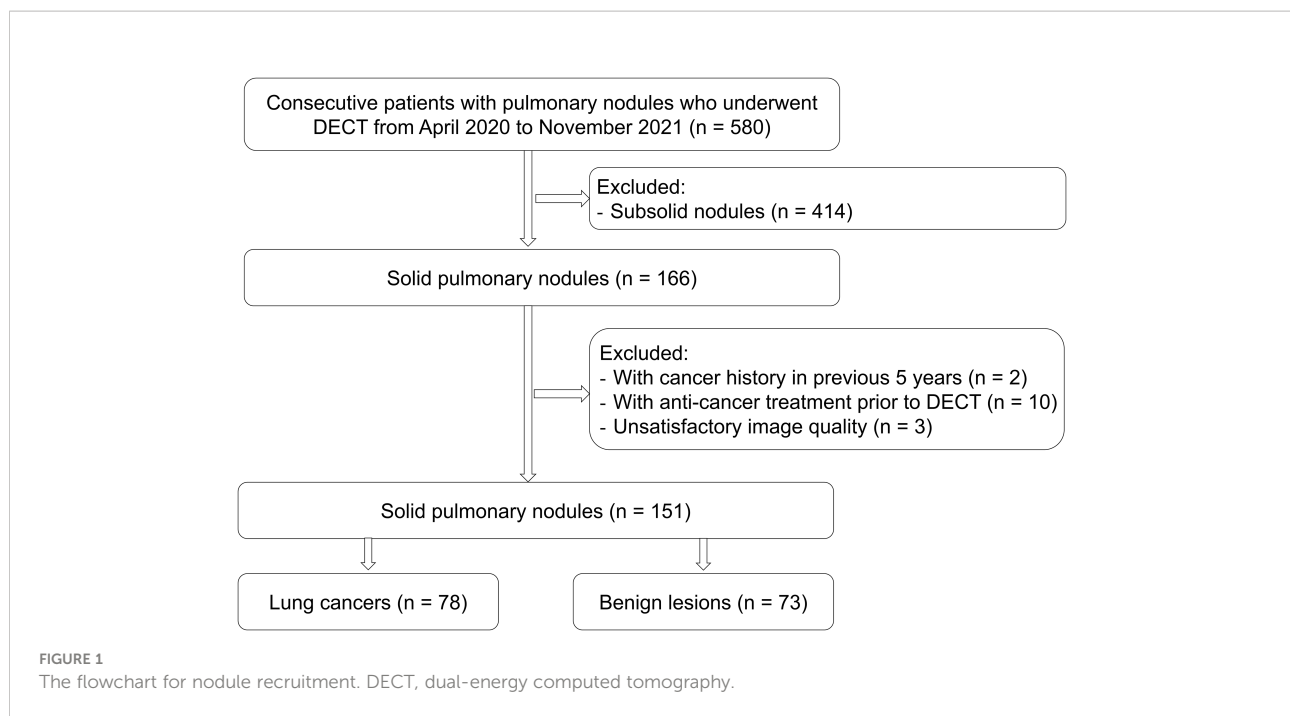
Granulomas are caused by mycobacterium tuberculosis, cryptococcus neoformans, and other unspecified conditions. Benign tumors include sclerosing pneumocytoma, hamartoma, and bronchial adenoma. Other benign entities include intrapulmonary lymph node and fibroplasia. Lung-RADS, Lung CT Screening Reporting and Data System; Zeff\_A, effective atomic number in arterial phase; IC\_A, iodine concentration in arterial phase; NIC\_A, normalized iodine concentration in arterial phase; Zeff\_V, effective atomic number in venous phase; IC\_V, iodine concentration in venous phase; NIC\_V, normalized iodine concentration in venous phase.

flow rate. The arterial phase was automatically triggered 5 s after the predetermined threshold (100 HU) was reached in a region of interest (ROI) that was placed at the ascending aorta at the layer of the pulmonary trunk. The venous phase was scanned 30 seconds after the arterial phase.

The same acquisition and reconstruction parameters in arterial and venous phases were used: tube voltage, 80/Sn140 kV; reference current, 205/87 mAs; pitch, 0.55; rotation time, 0.28 seconds; collimation, 64 × 0.6 mm; field of view, 350 × 350 mm; iterative reconstruction algorithm, SAFIRE (Strength level 4, Siemens Healthcare); reconstruction kernel, Q30f; matrix, 512 × 512; slice thickness, 0.5 mm; slice increment, 0.5 mm. Automated tube current modulation (CARE Dose 4D, Siemens Healthcare) was applied.

## Image analysis

The virtual non-enhanced image (VNI) was firstly obtained using arterial phase of DECT on a commercially available workstation (SyngoVia VB20, Siemens Healthcare). Second, all solid pulmonary nodules were automatically detected, segmented, and measured on the VNI using the uAI platform (United Imaging Healthcare, Shanghai, China), which is an artificial intelligence software based on deep learning method (24, 25). The segmentation results were assessed by two thoracic radiologists (JL and HQ, with 6 years and 11 years of experience) in the lung window (level - 500 HU, width 1500 HU). No manual adjustments of the segmentation results were conducted to avoid inter- and intra-observer variability, as all the segmentation results were satisfactory



to both radiologists. Third, the diameter and volume were recorded. The diameter was the average of the maximal long-axis diameter and the perpendicular diameter on the maximum transverse plane of the nodule. The volume was calculated by multiplying the number of voxels by the unit volume of a voxel. Fourth, both radiologists (JL and HQ), who were blinded to histopathological results, were encouraged to categorize all the solid pulmonary nodules according to Lung-RADS (version 1.1) (26). As the category 4X required subjective assessment, the cases of disagreement between the two radiologists were resolved by consulting a third thoracic radiologist with 26 years of experience (PZ). All the solid pulmonary nodules were finally categorized into 2, 3, 4A, 4B, and 4X according to the Lung-RADS basing on diameter and volume respectively.

The dual-phase DECT quantitative parameters were acquired on the same workstation. To minimize the variations caused by the patient's circulation status, the circular ROIs were placed in the nodules and the aorta at the same layer on axial slice by a radiologist (PZ). The ROIs were drawn at the site that best characterized the nodules as large as possible on the axial slice showing the maximum diameter, avoiding necrosis and adjacent pulmonary vessels and bronchi. The  $Z_{eff}$ , IC of nodule, and IC of aorta were measured. The NIC was calculated with the following formula:  $NIC = IC \text{ of nodule} / IC \text{ of aorta} \times 100\%$  (27). A total of 6 quantitative parameters were finally recorded, including  $Z_{eff}$  in arterial phase ( $Z_{eff\_A}$ ), IC in arterial phase ( $IC\_A$ ), NIC in arterial phase ( $NIC\_A$ ),  $Z_{eff}$  in venous phase ( $Z_{eff\_V}$ ), IC in venous phase ( $IC\_V$ ), and NIC in venous

phase ( $NIC\_V$ ). The representative DECT images of solid pulmonary nodules are shown in Figure 2.

## Statistical analysis

Statistical analysis was performed using SPSS (version 25.0; IBM Corp., Armonk, N.Y., USA), Medcalc (version 18.2.1; MedCalc, Ostend, Belgium), and R (version 4.0.3; The R Foundation for Statistical Computing, Vienna, Austria). The categorical variables were analyzed using Fisher's exact test, and the continuous variables were analyzed using independent sample *t*-test. Independent factors for differentiating lung cancers from benign solid pulmonary nodules were identified by inputting the significant variables using univariate logistic regression analysis. Then, multivariable logistic regression with backward stepwise selection and Akaike's information criterion was applied to construct the combined model basing on these significant independent factors (28). The area under curve (AUC) of the receiver operating characteristic (ROC) curve was used to evaluate the diagnostic performance. The binomial exact method was used to determine the confidence interval (CI) of AUC. The optimal cutoff threshold was delimited according to Youden's index of ROC analysis, and the corresponding sensitivity and specificity were also calculated. The DeLong test was used to compare the AUCs among the significant independent factors and the combined

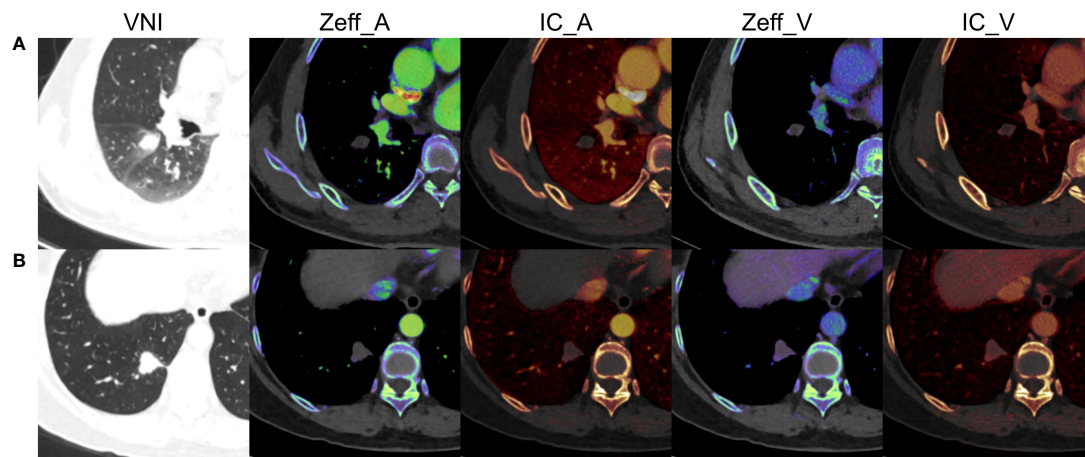


FIGURE 2

The representative dual-energy computed tomography images of solid pulmonary nodules. (A) A 49-year-old male with inflammation, diameter = 14.9 mm, volume = 1.949 cm<sup>3</sup>, Zeff\_A = 7.57, IC\_A = 0.10 mg/mL, NIC\_A = 1.15%, Zeff\_V = 7.80, IC\_V = 0.50 mg/mL, NIC\_V = 10.00%. (B) A 66-year-old female with adenocarcinomas, diameter = 18.8 mm, volume = 3.832 cm<sup>3</sup>, Zeff\_A = 8.19, IC\_A = 1.30 mg/mL, NIC\_A = 10.92%, Zeff\_V = 8.33, IC\_V = 1.70 mg/mL, NIC\_V = 27.42%. VNI, virtual non-enhanced images; Zeff\_A, effective atomic number in arterial phase; IC\_A, iodine concentration in arterial phase; NIC\_A, normalized iodine concentration in arterial phase; Zeff\_V, effective atomic number in venous phase; IC\_V, iodine concentration in venous phase; NIC\_V, normalized iodine concentration in venous phase.

model (29). Further comparisons of sensitivity and specificity were performed using the McNemar test (30). A two-tailed *P*-value < 0.05 was considered statistically significant.

## Results

### Clinical characteristics and nodule size

No significant differences of gender (*P* = 0.194) and age (*P* = 0.189) were found between lung cancers and benign solid pulmonary nodules. The diameter and volume of lung cancers were higher than that of benign solid pulmonary nodules (*P* = 0.013 and 0.036). The Lung-RADS categorization of diameter was different between groups (*P* = 0.008) while that of volume was not (*P* = 0.050) (Table 1).

### Quantitative parameters of DECT

Lung cancers showed higher Zeff\_A (8.07 ± 0.68 vs. 7.73 ± 0.49), IC\_A (1.43 ± 0.86 vs. 0.59 ± 1.43), and NIC\_A (13.46 ± 8.25 vs. 5.54 ± 13.28) than benign solid pulmonary nodules in arterial phase. (*P* = 0.001 or *P* < 0.001). In venous phase, lung cancers also showed higher Zeff\_V (8.42 ± 0.56 vs. 7.84 ± 1.01), IC\_V (2.03 ± 0.76 vs. 0.68 ± 0.97), and NIC\_V (36.74 ± 13.49 vs. 11.92 ± 17.85) than benign solid pulmonary nodules (all *P* < 0.001) (Table 1).

### Univariate and multivariable analyses

Univariate logistic regression analysis showed that diameter, Lung-RADS categorization of diameter, volume, Zeff\_A, IC\_A, NIC\_A, Zeff\_V, IC\_V, and NIC\_V were independent factors for differentiating lung cancers from benign solid pulmonary nodules (all *P* < 0.05) (Table 2).

Multivariable logistic regression showed the diameter and NIC\_V were significant predicting factors (Table 2). The calculation formula for the combined model was as follows:  $\ln(P/1-P) = -4.473 + 0.117 \times \text{diameter} + 0.111 \times \text{NIC}_V$ , where *P* is the probability of lung cancer (cutoff > 0.342).

### Diagnostic performance comparison

The IC\_V, NIC\_V, and combined model showed good diagnostic performance with AUCs of 0.891 (95% CI, 0.830 - 0.936), 0.888 (95% CI, 0.826 - 0.933), and 0.893 (95% CI, 0.832 - 0.937), and no significant differences of AUCs were found among them (Table 3 and Figure 3). Using the cutoff values of 0.95 mg/mL, 17.98%, and 0.342, the IC\_V, NIC\_V, and combined model yielded excellent sensitivity (0.987, 0.974, and 0.974) and good specificity (0.753, 0.781, and 0.781) (Table 2).

The AUCs of IC\_V, NIC\_V, and combined model were higher than those of diameter, Lung-RADS categorization of diameter, volume, Zeff\_A, and Zeff\_V (all *P* < 0.001). The AUC of IC\_V was also higher than that of IC\_A (*P* = 0.038). There were no significant

TABLE 2 Univariate and multivariable logistic regression analysis for predictive factors.

|                           | OR (95% CI)            | P       | AUC (95% CI)          | Sensitivity | Specificity | Cutoff  |
|---------------------------|------------------------|---------|-----------------------|-------------|-------------|---------|
| Univariate                |                        |         |                       |             |             |         |
| Diameter (mm)             | 1.069 (1.013 - 1.127)  | 0.014   | 0.626 (0.544 - 0.703) | 0.603       | 0.658       | > 15.3  |
| Lung-RADS (diameter)      | 2.023 (1.279 - 3.200)  | 0.003   | 0.643 (0.561 - 0.719) | 0.615       | 0.644       | > 4A    |
| Volume (cm <sup>3</sup> ) | 1.099 (1.004 - 1.202)  | 0.040   | 0.621 (0.539 - 0.699) | 0.615       | 0.644       | > 2.173 |
| Zeff_A                    | 3.542 (1.658 - 7.570)  | 0.001   | 0.721 (0.642 - 0.791) | 0.641       | 0.753       | > 7.98  |
| IC_A (mg/mL)              | 2.684 (1.708 - 4.218)  | < 0.001 | 0.821 (0.750 - 0.878) | 0.705       | 0.822       | > 0.95  |
| NIC_A (%)                 | 1.108 (1.056 - 1.162)  | < 0.001 | 0.829 (0.760 - 0.886) | 0.692       | 0.849       | > 9.81  |
| Zeff_V                    | 4.929 (2.406 - 10.097) | < 0.001 | 0.764 (0.689 - 0.830) | 0.897       | 0.630       | > 8.03  |
| IC_V (mg/mL)              | 6.860 (3.716 - 12.662) | < 0.001 | 0.891 (0.830 - 0.936) | 0.987       | 0.753       | > 0.95  |
| NIC_V (%)                 | 1.113 (1.076 - 1.151)  | < 0.001 | 0.888 (0.826 - 0.933) | 0.974       | 0.781       | > 17.98 |
| Multivariable             |                        |         |                       |             |             |         |
| Diameter (mm)             | 1.124 (1.040 - 1.214)  | 0.003   | 0.893 (0.832 - 0.937) | 0.974       | 0.781       | 0.342   |
| NIC_V (%)                 | 1.117 (1.080 - 1.156)  | < 0.001 |                       |             |             |         |

OR, odds ratio; AUC, area under curve; CI, confidence intervals; Lung-RADS, Lung CT Screening Reporting and Data System; Zeff\_A, effective atomic number in arterial phase; IC\_A, iodine concentration in arterial phase; NIC\_A, normalized iodine concentration in arterial phase; Zeff\_V, effective atomic number in venous phase; IC\_V, iodine concentration in venous phase; NIC\_V, normalized iodine concentration in venous phase.

differences of AUCs between IC\_V and NIC\_A ( $P = 0.051$ ), between NIC\_V and IC\_A ( $P = 0.053$ ), between NIC\_V and NIC\_A ( $P = 0.066$ ), between combined model and IC\_A ( $P = 0.062$ ), and between combined model and NIC\_A ( $P = 0.079$ ) (Table 3).

Further comparisons of sensitivity and specificity were performed between IC\_V, NIC\_V, combined model and IC\_A, NIC\_A. The results of McNemar test showed that the sensitivities of IC\_V, NIC\_V, and combined model were higher than those of IC\_A and NIC\_A (all  $P < 0.001$ ), while there were no significant differences of specificities (all  $P > 0.05$ ) (Table 4).

## Discussion

Our study explored the diagnosis performance of quantitative parameters of DECT and nodule size in distinguishing lung cancers

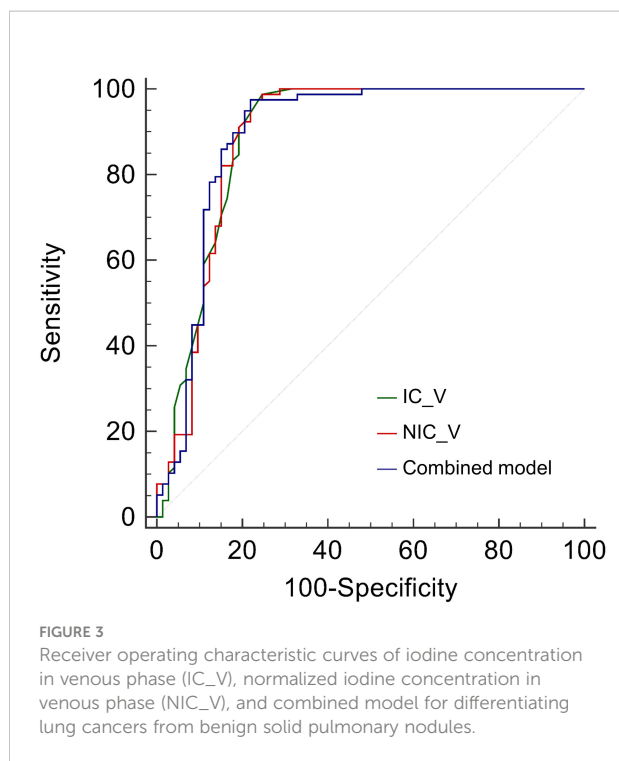
from benign lesions in solid pulmonary nodules. The IC\_V, NIC\_V, and combined model consisting of diameter and NIC\_V showed good diagnostic performance and outperformed the nodule size, Lung-RADS, Zeff\_A, Zeff\_V, IC\_A, and NIC\_A. The combined model did not increase the diagnostic performance compared with IC\_V or NIC\_V. These results indicated that the differentiation of lung cancers from benign lesions in solid pulmonary nodules was feasible using DECT-derived IC\_V or NIC\_V alone.

In recent years, DECT is an emerging diagnostic technology with various clinical applications, especially in thoracic imaging (31–33). IC, the most commonly used quantitative parameter of DECT, is considered to be equivalent to the actual value of enhancement. The enhancement of malignant nodules is associated perfusion and permeability of the capillaries, reflecting the underlying microvessel density and tumor angiogenesis (34, 35). The iodine parameters from DECT were

TABLE 3 Comparisons of area under curves among predictive factors.

| Predictive factors   | P1      | P2      | P3      |
|----------------------|---------|---------|---------|
| Diameter             | < 0.001 | < 0.001 | < 0.001 |
| Lung-RADS (diameter) | < 0.001 | < 0.001 | < 0.001 |
| Volume               | < 0.001 | < 0.001 | < 0.001 |
| Zeff_A               | < 0.001 | < 0.001 | < 0.001 |
| IC_A                 | 0.038   | 0.053   | 0.062   |
| NIC_A                | 0.051   | 0.066   | 0.079   |
| Zeff_V               | < 0.001 | < 0.001 | < 0.001 |
| IC_V                 | –       | 0.696   | 0.869   |
| NIC_V                | 0.696   | –       | 0.633   |
| Combined model       | 0.869   | 0.633   | –       |

P1 = P values between IC\_V and the others; P2 = P values between NIC\_V and the others; P3 = P values between combined model and the others. Lung-RADS, Lung CT Screening Reporting and Data System; Zeff\_A, effective atomic number in arterial phase; IC\_A, iodine concentration in arterial phase; NIC\_A, normalized iodine concentration in arterial phase; Zeff\_V, effective atomic number in venous phase; IC\_V, iodine concentration in venous phase; NIC\_V, normalized iodine concentration in venous phase.



significantly correlated with perfusion CT parameters with lower radiation exposure and contrast agent usage, which were considered surrogate measures for vascularity and perfusion (14, 36, 37). We found the lung cancers accumulated more iodine than benign solid nodules, which was consistent with previous reports (15, 17–19). Zeff quantitatively represents the composite atom for a compound or mixture of various materials (32). González-Pérez et al. found lower Zeff correlated with malignant pulmonary lesions, which was contrary to our result (38). The potential reason might be the different distribution of histologic subtypes in the included pulmonary lesions (39). Further study with large sample is needed to address this issue in the future.

This study also compared the diagnostic performance of iodine parameters and Zeff in differentiating lung cancers from

benign lesions in solid pulmonary nodules. Our results showed that the IC\_V and NIC\_V had higher AUCs than Zeff\_A and Zeff\_V, and had superior sensitivities than IC\_A and NIC\_A, which was similar to previous studies (16, 17). Generally, the iodine contrast agent can easily leak into the intercellular space in lung cancer, due to angiogenesis, loose capillary endothelial cells, and incomplete basement membranes. Besides, the microvessels are tortuous in lung cancer, and the contrast agent flows slowly. In arterial phase, the microvessels cannot be full of the contrast agent, but the contrast agent can fill the microvessels and penetrate into the intercellular space in venous phase (40). Therefore, the IC\_V was higher than IC\_A in lung cancers ( $t = 7.919, P < 0.001$ ) but not in benign lesions ( $t = 0.529, P = 0.598$ ) in our study. Recent study of DECT also used radiomic features from virtual monoenergetic image to differentiate benign from malignant pulmonary nodules (41). However, the complexity of this approach limited its integration into the clinical workflow as it required additional software (37).

The Lung-RADS (version 1.1) introduced volume to stratify the malignant risk of pulmonary nodule (42–44). Thus both the Lung-RADS of diameter and volume were used to categorize the solid pulmonary nodules in this study. The AUCs of nodule size and Lung-RADS categorization ranged from 0.621 to 0.643, and were lower than that of IC\_V and NIC\_V. These results indicated that the nodule size and Lung-RADS categorization had inadequate diagnostic efficiency. Besides, the combined model integrating nodule diameter and NIC\_V did not significantly improve the diagnostic efficiency compared with IC\_V or NIC\_V. Therefore, using the IC\_V or NIC\_V alone enabled diagnostic utility in the differentiation between lung cancers and benign lesions in solid pulmonary nodules.

The current management guidelines of pulmonary nodules in lung cancer screening recommend follow-up CT at 3 months, positron emission tomography/computed tomography (PET/CT), or tissue sampling for solid nodules over 8 mm (7, 26, 45). Although PET/CT provides more metabolic information than CT alone, this modality is associated with excessive radiation dose and high cost. The transthoracic needle biopsy and bronchoscopy, as invasive tissue sampling approaches, are

TABLE 4 Comparisons of sensitivity and specificity.

| Comparisons              | Sensitivity |         | Specificity |       |
|--------------------------|-------------|---------|-------------|-------|
|                          | $\chi^2$    | P       | $\chi^2$    | P     |
| IC_V vs. IC_A            | 20.045      | < 0.001 | 1.231       | 0.267 |
| NIC_V vs. IC_A           | 17.391      | < 0.001 | 0.364       | 0.549 |
| Combined model vs. IC_A  | 16.000      | < 0.001 | 0.308       | 0.581 |
| IC_V vs. NIC_A           | 21.043      | < 0.001 | 2.400       | 0.118 |
| NIC_V vs. NIC_A          | 18.375      | < 0.001 | 1.231       | 0.267 |
| Combined model vs. NIC_A | 16.962      | < 0.001 | 1.231       | 0.267 |

IC\_A, iodine concentration in arterial phase; NIC\_A, normalized iodine concentration in arterial phase; IC\_V, iodine concentration in venous phase; NIC\_V, normalized iodine concentration in venous phase.

often selected based on location of the nodule, clinical expertise, comorbidities, and physical condition of patients. Previous studies showed transthoracic needle biopsy had a higher pooled diagnostic than bronchoscopy, but was associated with an increased risk for pneumothorax and hemorrhage (46, 47). Therefore, the DECT may be alternative in the follow-up CT for further assessment of solid pulmonary nodules as the IC\_V and NIC\_V have diagnostic utility in distinguishing lung cancers from benign lesions.

There are several limitations in this study. First, this was a single center study with a relatively small sample size, further external validation datasets are needed to test the replicability of our results. Second, the nodule size was assessed using VNI other than true non-enhanced image. A phantom study of lung tumor model found that VNI could be alternative to true non-enhanced image in volumetry (48). Third, comprehensive morphological characteristics were not included in this study. The combination of morphological and quantitative features may improve the diagnostic performance, and further study is needed. Fourth, we did not study the intermediate nodules separately and the subsolid nodules were also excluded. The adding value of the IC\_V and NIC\_V to those nodules and Lung-RADS needs more researches.

In conclusion, the DECT-derived IC\_V and NIC\_V had good diagnostic performance in differentiation of lung cancers from benign lesions, and could be a non-invasive biomarker to predict malignant risk of solid pulmonary nodules in clinical practice.

## Data availability statement

The original contributions presented in the study are included in the article/supplementary material. Further inquiries can be directed to the corresponding author.

## Ethics statement

The studies involving human participants were reviewed and approved by the Institutional Review Board of Sichuan Cancer

Hospital. The patients/participants provided their written informed consent to participate in this study.

## Author contributions

CH, JL, and PZ conceived and designed the study. YL, LL, HQ, LG, and SH collected the data. CH and JL analyzed the data and drafted the manuscript. All authors reviewed the manuscript and PZ revised the final manuscript. JL, LG, and PZ provided funding for the study. All authors contributed to the article and approved the submitted version.

## Funding

This study was supported by the National Natural Science Foundation of China (grant number 82202141), the Sichuan Science and Technology Program (grant numbers 2021YFS0075, 2021YFS0225), the Chengdu Science and Technology Program (grant number 2021-YF05-01507-SN), and the Beijing Medical Award Funding (grant number YXJL-2022-0105-0143).

## Conflict of interest

The authors declare that the research was conducted in the absence of any commercial or financial relationships that could be construed as a potential conflict of interest.

## Publisher's note

All claims expressed in this article are solely those of the authors and do not necessarily represent those of their affiliated organizations, or those of the publisher, the editors and the reviewers. Any product that may be evaluated in this article, or claim that may be made by its manufacturer, is not guaranteed or endorsed by the publisher.

## References

1. Siegel RL, Miller KD, Fuchs HE, Jemal A. Cancer statistics, 2022. *CA Cancer J Clin* (2022) 72:7–33. doi: 10.3322/caac.21708
2. Global Burden of Disease Cancer C. Cancer incidence, mortality, years of life lost, years lived with disability, and disability-adjusted life years for 29 cancer groups from 2010 to 2019: A systematic analysis for the global burden of disease study 2019. *JAMA Oncol* (2021) 8:420–44. doi: 10.1001/jamaoncol.2021.6987
3. Zhang S, Sun K, Zheng R, Zeng H, Wang S, Chen R, et al. Cancer incidence and mortality in China, 2015. *J Natl Cancer Center* (2021) 1:2–11. doi: 10.1016/j.jncc.2020.12.001
4. Silva M, Milanese G, Ledda RE, Pastorino U, Sverzellati N. Screen-detected solid nodules: from detection of nodule to structured reporting. *Transl Lung Cancer Res* (2021) 10:2335–46. doi: 10.21037/tlcr-20-296
5. Gierada DS, Rydzak CE, Zei M, Rhea L. Improved interobserver agreement on lung-RADS classification of solid nodules using semiautomated CT volumetry. *Radiology* (2020) 297:675–84. doi: 10.1148/radiol.2020200302
6. Sundaram V, Gould MK, Nair VS. A comparison of the PanCan model and lung-RADS to assess cancer probability among people with screening-detected, solid lung nodules. *Chest* (2021) 159:1273–82. doi: 10.1016/j.chest.2020.10.040
7. MacMahon H, Naidich DP, Goo JM, Lee KS, Leung ANC, Mayo JR, et al. Guidelines for management of incidental pulmonary nodules detected on CT images: From the Fleischner society 2017. *Radiology* (2017) 284:228–43. doi: 10.1148/radiol.2017161659
8. Mendoza DP, Petranovic M, Som A, Wu MY, Park EY, Zhang EW, et al. Lung-RADS category 3 and 4 nodules on lung cancer screening in clinical practice. *AJR Am J Roentgenol* (2022) 219:55–65. doi: 10.2214/AJR.21.27180

9. Liu J, Xu H, Qing H, Li Y, Yang X, He C, et al. Comparison of radiomic models based on low-dose and standard-dose CT for prediction of adenocarcinomas and benign lesions in solid pulmonary nodules. *Front Oncol* (2020) 10:634298. doi: 10.3389/fonc.2020.634298
10. Hammer MM, Hunsaker AR. Strategies for reducing false-positive screening results for intermediate-size nodules evaluated using lung-RADS: A secondary analysis of national lung screening trial data. *AJR Am J Roentgenol* (2022) 219:397-405. doi: 10.2214/AJR.22.27595
11. Gould MK, Donington J, Lynch WR, Mazzone PJ, Midthun DE, Naidich DP, et al. Evaluation of individuals with pulmonary nodules: when is it lung cancer? diagnosis and management of lung cancer, 3rd ed: American college of chest physicians evidence-based clinical practice guidelines. *Chest* (2013) 143:e93S-e120S. doi: 10.1378/chest.12-2351
12. Beig N, Khorrami M, Alilou M, Prasanna P, Braman N, Orooji M, et al. Perinodular and intranodular radiomic features on lung CT images distinguish adenocarcinomas from granulomas. *Radiology* (2019) 290:783-92. doi: 10.1148/radiol.2018180910
13. Feng B, Chen X, Chen Y, Lu S, Liu K, Li K, et al. Solitary solid pulmonary nodules: a CT-based deep learning nomogram helps differentiate tuberculosis granulomas from lung adenocarcinomas. *Eur Radiol* (2020) 30:6497-507. doi: 10.1007/s00330-020-07024-z
14. Goo HW, Goo JM. Dual-energy CT: New horizon in medical imaging. *Korean J Radiol* (2017) 18:555-69. doi: 10.3348/kjr.2017.18.4.555
15. Wang G, Zhang C, Li M, Deng K, Li W. Preliminary application of high-definition computed tomographic gemstone spectral imaging in lung cancer. *J Comput Assist Tomogr* (2014) 38:77-81. doi: 10.1097/RCT.0b013e3182a21633
16. Hou WS, Wu HW, Yin Y, Cheng JJ, Zhang Q, Xu JR. Differentiation of lung cancers from inflammatory masses with dual-energy spectral CT imaging. *Acad Radiol* (2015) 22:337-44. doi: 10.1016/j.acra.2014.10.004
17. Zhang Y, Cheng J, Hua X, Yu M, Xu C, Zhang F, et al. Can spectral CT imaging improve the differentiation between malignant and benign solitary pulmonary nodules? *PLoS One* (2016) 11:e0147537. doi: 10.1371/journal.pone.0147537
18. Reiter MJ, Winkler WT, Kagy KE, Schwoppe RB, Lisanti CJ. Dual-energy computed tomography for the evaluation of enhancement of pulmonary nodules  $\leq$  3 cm in size. *J Thorac Imaging* (2017) 32:189-97. doi: 10.1097/RTI.0000000000000263
19. Zhu B, Zheng S, Jiang T, Hu B. Evaluation of dual-energy and perfusion CT parameters for diagnosing solitary pulmonary nodules. *Thorac Cancer* (2021) 12:2691-7. doi: 10.1111/1759-7714.14105
20. She Y, Zhao L, Dai C, Ren Y, Jiang G, Xie H, et al. Development and validation of a nomogram to estimate the pretest probability of cancer in Chinese patients with solid solitary pulmonary nodules: A multi-institutional study. *J Surg Oncol* (2017) 116:756-62. doi: 10.1002/jso.24704
21. Yang W, Sun Y, Fang W, Qian F, Ye J, Chen Q, et al. High-resolution computed tomography features distinguishing benign and malignant lesions manifesting as persistent solitary subsolid nodules. *Clin Lung Cancer* (2018) 19:e75-83. doi: 10.1016/j.clcc.2017.05.023
22. Son JY, Lee HY, Kim JH, Han J, Jeong JY, Lee KS, et al. Quantitative CT analysis of pulmonary ground-glass opacity nodules for distinguishing invasive adenocarcinoma from non-invasive or minimally invasive adenocarcinoma: the added value of using iodine mapping. *Eur Radiol* (2016) 26:43-54. doi: 10.1007/s00330-015-3816-y
23. Yang Y, Li K, Sun D, Yu J, Cai Z, Cao Y, et al. Invasive pulmonary adenocarcinomas versus preinvasive lesions appearing as pure ground-glass nodules: Differentiation using enhanced dual-source dual-energy CT. *AJR Am J Roentgenol* (2019) 213:W114-W122. doi: 10.2214/AJR.19.21245
24. Mu G, Chen Y, Wu D, Zhan Y, Zhou XS, Gao Y. *Relu cascade of feature pyramid networks for CT pulmonary nodule detection*. Springer International Publishing Cham (2019) p. 444-52. doi: 10.1007/978-3-030-32692-0\_51
25. Wang Q, Zhou X, Wang C, Liu Z, Huang J, Zhou Y, et al. WGAN-based synthetic minority over-sampling technique: Improving semantic fine-grained classification for lung nodules in CT images. *IEEE Access* (2019) 7:18450-63. doi: 10.1109/ACCESS.2019.2896409
26. American College of Radiology. *Lung CT screening reporting and data system (Lung-RADS, version 1.1)* (2019). Available at: <https://www.acr.org/Clinical-Resources/Reporting-and-Data-Systems/Lung-Rads>.
27. Ha T, Kim W, Cha J, Lee YH, Seo HS, Park SY, et al. Differentiating pulmonary metastasis from benign lung nodules in thyroid cancer patients using dual-energy CT parameters. *Eur Radiol* (2022) 32:1902-11. doi: 10.1007/s00330-021-08278-x
28. Pan W. Akaike's information criterion in generalized estimating equations. *Biometrics* (2001) 57:120-5. doi: 10.1111/j.0006-341x.2001.00120.x
29. DeLong ER, DeLong DM, Clarke-Pearson DL. Comparing the areas under two or more correlated receiver operating characteristic curves: a nonparametric approach. *Biometrics* (1988) 44:837-45. doi: 10.2307/2531595
30. Hawass NE. Comparing the sensitivities and specificities of two diagnostic procedures performed on the same group of patients. *Br J Radiol* (1997) 70:360-6. doi: 10.1259/bjr.70.832.9166071
31. Odio EG, Truong MT, Duran C, de Groot PM, Godoy MC. Role of dual-energy computed tomography in thoracic oncology. *Radiol Clin North Am* (2018) 56:535-48. doi: 10.1016/j.rcl.2018.03.011
32. Kim C, Kim W, Park SJ, Lee YH, Hwang SH, Yong HS, et al. Application of dual-energy spectral computed tomography to thoracic oncology imaging. *Korean J Radiol* (2020) 21:838-50. doi: 10.3348/kjr.2019.0711
33. Hamid S, Nasir MU, So A, Andrews G, Nicolaou S, Qamar SR. Clinical applications of dual-energy CT. *Korean J Radiol* (2021) 22:970-82. doi: 10.3348/kjr.2020.0996
34. Yi CA, Lee KS, Kim EA, Han J, Kim H, Kwon OJ, et al. Solitary pulmonary nodules: dynamic enhanced multi-detector row CT study and comparison with vascular endothelial growth factor and microvessel density. *Radiology* (2004) 233:191-9. doi: 10.1148/radiol.2331031535
35. Kawai T, Shibamoto Y, Hara M, Arakawa T, Nagai K, Ohashi K. Can dual-energy CT evaluate contrast enhancement of ground-glass attenuation? phantom and preliminary clinical studies. *Acad Radiol* (2011) 18:682-9. doi: 10.1016/j.acra.2010.12.014
36. Kang HJ, Kim SH, Bae JS, Jeon SK, Han JK. Can quantitative iodine parameters on DECT replace perfusion CT parameters in colorectal cancers? *Eur Radiol* (2018) 28:4775-82. doi: 10.1007/s00330-018-5502-3
37. Deniffel D, Sauter A, Fingerle A, Rummeny EJ, Makowski MR, Pfeiffer D. Improved differentiation between primary lung cancer and pulmonary metastasis by combining dual-energy CT-derived biomarkers with conventional CT attenuation. *Eur Radiol* (2021) 31:1002-10. doi: 10.1007/s00330-020-07195-9
38. Gonzalez-Perez V, Arana E, Barrios M, Bartres A, Cruz J, Montero R, et al. Differentiation of benign and malignant lung lesions: Dual-energy computed tomography findings. *Eur J Radiol* (2016) 85:1765-72. doi: 10.1016/j.ejrad.2016.07.019
39. Jia Y, Xiao X, Sun Q, Jiang H. CT spectral parameters and serum tumour markers to differentiate histological types of cancer histology. *Clin Radiol* (2018) 73:1033-40. doi: 10.1016/j.crad.2018.07.104
40. Zhang Z, Zou H, Yuan A, Jiang F, Zhao B, Liu Y, et al. A single enhanced dual-energy CT scan may distinguish lung squamous cell carcinoma from adenocarcinoma during the venous phase. *Acad Radiol* (2020) 27:624-9. doi: 10.1016/j.acra.2019.07.018
41. Liang G, Yu W, Liu SQ, Xie MG, Liu M. The value of radiomics based on dual-energy CT for differentiating benign from malignant solitary pulmonary nodules. *BMC Med Imaging* (2022) 22:95. doi: 10.1186/s12880-022-00824-3
42. Chelala L, Hossain R, Kazerooni EA, Christensen JD, Dyer DS, White CS. Lung-RADS version 1.1: Challenges and a look ahead, from the AJR special series on radiology reporting and data systems. *AJR Am J Roentgenol* (2021) 216:1411-22. doi: 10.2214/AJR.20.24807
43. Nishino M. CT volumetry for lung-RADS classification of solid nodules. *Radiology* (2020) 297:685-6. doi: 10.1148/radiol.2020203298
44. Silva M, Milanese G, Sestini S, Sabia F, Jacobs C, van Ginneken B, et al. Lung cancer screening by nodule volume in lung-RADS v1.1: negative baseline CT yields potential for increased screening interval. *Eur Radiol* (2021) 31:1956-68. doi: 10.1007/s00330-020-07275-w
45. Mazzone PJ, Silvestri GA, Souter LH, Caverly TJ, Kanne JP, Katki HA, et al. Screening for lung cancer: CHEST guideline and expert panel report. *Chest* (2021) 160:e427-94. doi: 10.1016/j.chest.2021.06.063
46. Han Y, Kim HJ, Kong KA, Kim SJ, Lee SH, Ryu YJ, et al. Diagnosis of small pulmonary lesions by transbronchial lung biopsy with radial endobronchial ultrasound and virtual bronchoscopic navigation versus CT-guided transthoracic needle biopsy: A systematic review and meta-analysis. *PLoS One* (2018) 13:e0191590. doi: 10.1371/journal.pone.0191590
47. Folch EE, Labarca G, Ospina-Delgado D, Kheir F, Majid A, Khandhar SJ, et al. Sensitivity and safety of electromagnetic navigation bronchoscopy for lung cancer diagnosis: Systematic review and meta-analysis. *Chest* (2020) 158:1753-69. doi: 10.1016/j.chest.2020.05.534
48. Hering DA, Kroger K, Bauer RW, Eich HT, Haverkamp U. Comparison of virtual non-contrast dual-energy CT and a true non-contrast CT for contouring in radiotherapy of 3D printed lung tumour models in motion: a phantom study. *Br J Radiol* (2020) 93:20200152. doi: 10.1259/bjr.20200152